Hydrothermal assembly of micro-nano-integrated core-sheath carbon fibers for high-performance all-carbon micro-supercapacitors

*Shengli Zhai, H. Enis Karahan, Li Wei, Xuncai Chen, Zheng Zhou, Xin Wang, and Yuan Chen**

Mr. S. Zhai, Dr. L. Wei, Mr. X. Chen, Mr. Z. Zhou, Prof. Y. Chen
The University of Sydney
School of Chemical and Biomolecular Engineering
Sydney, New South Wales 2006, Australia
E-mail: yuan.chen@sydney.edu.au

Mr. S. Zhai, Mr. H. E. Karahan, Prof. X. Wang
Nanyang Technological University
School of Chemical and Biomedical Engineering
62 Nanyang Drive, 637459, Singapore

Abstract

Wearable electronic devices (WED) require flexible, stable, and long-lasting power sources for their ever-expanding functionalities. Fiber-based micro-supercapacitors (FMSCs) are promising power solutions for novel WEDs because of their mechanical flexibility, small size and good integrability. Various porous carbon fibers have been explored as electrodes for FMSCs. However, current FMSCs often show poor rate capability due to modest electrical conductivity in fiber electrodes. Here, we demonstrate the synthesis of a micro-nano-integrated core-sheath fiber comprised of a microscale core made of commercial graphite fibers and a nanoscale hybrid sheath comprised of nitrogen doped graphene oxide sheets and multi-walled carbon nanotubes. The graphite fiber core provides fast electron transfer pathways, while the high surface area nano-hybrid sheath enables efficient capacitive energy storage. The core-sheath fiber achieves more than six times increases in capacitance retention compared to hybrid carbon fibers without the conductive core. Solid-state FMSCs were assembled using the core-sheath fibers as electrodes, which concurrently possess high length

capacitance (12.8 mF cm^{-1}) and volumetric capacitance (27 F cm^{-3}), showing an energy density of 3.75 mWh cm^{-3} and a power density of 612 mW cm^{-3}. Furthermore, multiple FMSCs can be easily assembled into flexible energy storage units with expanded voltage and current windows, demonstrating good potential for practical WED applications.

Keywords

Carbon fiber; supercapacitor; wearable electronics; graphene oxide; carbon nanotube

1. Introduction

With the emergence of trendy devices, such as Google glass, Apple watch, Fitbit wristband, and Oculus VR headset, wearable electronic devices (WEDs) already became a reality rather than science fiction [1, 2]. As there is no other reliable alternatives that offer stable and long-lasting energy supply, small Li-ion batteries serve as the main energy storage solution for WEDs. However, batteries often suffer from sluggish charge/discharge rate and low power density [3-5]. In addition to these, common batteries are also limited in mechanical flexibility, which restricts the innovation of WEDs [6-10]. Micro-supercapacitors (MSCs) are promising as alternative energy storage solutions for WEDs because of their high power density, fast charge/discharge rate, and long cycling life [4, 11-14]. Among various alternatives, being lightweight, highly flexible and one-dimensional (1D), fiber-based MSCs (FMCSs) attracted a great attention [15-18]. FMSCs also offer a great flexibility for design, as they are compatible with weaving and knitting. Further, they can facilitate the integration of WEDs with textiles and other fiber devices [15-18].

Fiber electrodes are the key components of FMSCs, and they should possess large surface area (for charge storage), high conductivity (for fast charging/discharging), and mechanical flexibility for building high-performance WEDs. Graphene based materials have been explored as building blocks to fabricate fiber electrodes [19-21], due to their large specific surface area (~2630 $m^2 g^{-1}$) [22], high electrical conductivity (up to 10^6 S cm^{-1}) [19], and high mechanical flexibility [23]. Several methods were used to assemble graphene-based materials into fiber electrodes, including wet-spinning [24-28], dry-spinning [14, 27, 29, 30], rolling graphene films into fibers [31-33], to name a few. However still, it is challenging to translate the excellent nanoscale properties of graphene-based materials into their macroscale assemblies. One reason is that graphene layers often restack together leading to small surface

area for charge storage. Also, the contact resistance among small individual graphene sheets results in low overall electrical conductivity.

We recently developed a versatile new approach, *i.e.* space-confined hydrothermal assembly, to convert nanoscale materials into microscale fibers using capillary channels [15, 29, 30]. Using this method, graphene oxide (GO) and carbon nanotubes were effectively assembled into porous hybrid fibers. The surface area of hybrid fibers reaches ~400 m^2 g^{-1}. However, their electrical conductivity undesirably remained below 100 S cm^{-1}. Particularly, with the increase of hybrid carbon fiber diameter from around 20 to above 200 μm, their electrical conductivity dropped to less than 20 S cm^{-1} [30]. It should be noted that electrodes with electrical low conductivity result in poor rate capability in SCs. The rate capability is a critical performance indicator for SCs since higher the rate capability wider the range of charge/discharge current densities with minor variation in capacitance, which is desirable for vast practical applications [34].

Previous studies have reported the integration of neat metal wires, such as Au, Pt, Ni, Ti, or metal-coated plastic fibers as current collectors into fiber electrodes for achieving high rate capability in FMSCs [35-38]. However, metal wires take up a considerable portion of the total weight and volume of FMSCs with limited contribution to the total device capacitance, which inevitably compromises the device gravimetric and volumetric energy/power density [4]. Commercial carbon (graphite) fibers comprise many graphite filaments of typically around 5-10 μm in diameter, and importantly they have high electrical conductivity (up to 10^4 S cm^{-1}) with excellent mechanical properties [39]. Further, the density of graphite fibers (*i.e.* ~1.7 g cm^{-3}) is around one tenth of the density of metal wires (*e.g.* Au is at around 20 g cm^{-3}) [35, 40]. They are commercially available at low cost. Thus, graphite fibers offer a good potential in creating practical fiber electrodes for FMSCs.

In this study, we describe the synthesis of micro-nano-integrated core-sheath fiber electrodes using the space-confined hydrothermal assembly method for solid-state all-carbon FMSCs. The "core-sheath" structures involve highly conductive microscale "cores" made of commercial graphite fibers and nanoscale porous "sheaths" comprised of the hybrid of nitrogen doped GO and multiple walled carbon nanotubes (MWCNTs). The fiber electrodes were assembled into solid-state FMSCs with high specific energy and power densities. Furthermore, multiple FMSCs were integrated as energy storage units to power light-emitting diodes (LEDs), unveiling their high potential for WED applications.

2. Experimental

2.1 Preparation of GO dispersions

The expandable graphite powder (DL50, Qingdao Henglide Graphite Co., Ltd) was first thermally expanded at 1050 °C for around 15 seconds to obtain expanded graphite. GO sheets were prepared through a modified Hummers' method using expanded graphite particles [25, 41, 42]. Briefly, the expanded graphite powder (1 g) and 200 mL H_2SO_4 (Merck, 98%) were added to a round bottom flask (500 mL), followed by the dropwise addition of $KMnO_4$ (5 g). Then the mixture was stirred at 30 ^oC for 24 hours. Afterwards, deionized (DI) water (200 mL) and H_2O_2 (50 mL) were added to the mixture in an ice-water bath under stirring for 30 minutes. Subsequently, the resulting brown colored slurry was washed *via* multiple cycles of centrifugation by HCl (1 M) and then with DI water until the pH of supernatant reaches above pH 5. Finally, the concentration of the GO dispersion was adjusted to 10 mg mL^{-1}.

2.2 Functionalization of MWCNTs and graphite fibers

MWCNTs (FloTube 9000, CNano Technology) of ~10 nm in diameter and typically ~10 μm in length were functionalized by refluxing in HNO_3 (65%) for 4 hours. Then, the functionalized MWCNTs were dispersed in DI water, and its concentration was adjusted to 2.5 mg mL^{-1}. Graphite fibers (Zoltek Panex 35) were first dipped into concentrated H_2SO_4 (98%) for 15 minutes. Next, they were sonicated in a mixture of acetone and ethanol for 15 minutes, followed by washing with DI water. Finally, treated graphite fibers were dried in vacuum oven at 30 °C before use.

2.3 Synthesis of micro-nano-integrated core-sheath fibers

The homogeneous GO/MWCNT dispersion at the mass ratio of 4:1 was prepared by mixing GO dispersion (10 mg mL^{-1}) and MWCNT dispersion (2.5 mg mL^{-1}) with the addition of ethylenediamine (EDA, 20 μL mL^{-1}). As illustrated in Fig. 1, the dispersion was injected into one side sealed glass tubes of 80 mm in length and 2 mm in inner diameter. At the same time, a bundle of graphite fibers (diameter: ~40-50 μm, length: ~10 cm, and electrical conductivity: 680 S cm^{-1}) were inserted into the glass tubes. Subsequently, the glass tubes were filled vertically in a stainless steel autoclave bomb lined by Teflon, and additional water was added in the autoclave outside of glass tubes. Lastly, resulting stuffed glass tubes, which can be considered space-confined hydrothermal mini-reactors, were subjected to heat at 180 ^{o}C for 12 hours. After cooling, the resulting core-sheath fibers were poured into a water reservoir; and then dried in open air at room temperature overnight. For comparison, GO/MWCNT/EDA-derived hybrid fibers without graphite fiber cores (in short, core-free hybrid fibers) were also synthesized.

2.4 Physicochemical characterization of fibers

The morphology of fibers was characterized by field-emission scanning electron microscope (SEM, JEOL, JSM-6701) at an electron accelerating voltage of 5 kV. X-ray photoelectron

spectroscopy (XPS, PHI Quantera) and energy dispersive X-ray spectroscopy (EDS, JEOL, JSM-6701) were employed to determine the chemical composition of fibers prepared. The electrical conductivity of fibers was measured using a four-point probe station (Keithley) with a probe pin diameter of 40.6 μm and the spacing between pins at 1.6 mm.

2.5 Electrochemical properties of fibers

The electrochemical properties of fibers were first evaluated by cyclic voltammetry (CV) and galvanostatic charge and discharge (GCD) on a chemical workstation (CHI 660E). The tests were carried out in a 3-electrode configuration in H_2SO_4 (1 M) electrolyte, using the core-sheath fibers (1 cm in length) as working electrodes, an Ag/AgCl (3 M KCl) electrode as the reference electrode, and a platinum electrode as the counter electrode. The capacitance of carbon fiber electrodes ($C_{electrode}$) was determined *via* CV and GCD according to equation (1) and (2), respectively.

$$C_{electrode} = \frac{Q}{2V} = \frac{1}{2Vv}\int_{V_-}^{V_+} i(V)dV \quad (1)$$

where Q is the total charge obtained by integrating the enclosed area of CV curves, V is the voltage window ($V = V_+ - V_-$), v is the scan rate of CV curves, and $i(V)$ is the current of CV curves.

$$C_{electrode} = i/(dV/dt) \quad (2)$$

i is the discharge current of GCD curves, t is the discharge time, and V is the voltage.

The specific volumetric capacitance ($C_{V,electrode}$) of the carbon fiber electrode was calculated using equation (3):

$$C_{V,electrode} = C_{electrode}/V_{electrode} \quad (3)$$

where $V_{electrode}$ is the volume of the carbon fiber electrode.

2.6 Fabrication of solid-state FMSCs

Symmetric FMSCs were fabricated using two fibers of the same length and diameter as electrodes in poly (vinyl alcohol) (PVA)/H_3PO_4 gel electrolyte. Two fiber electrodes were placed in parallel on a polyethylene terephthalate (PET) film with one end of the fiber attached to a conductive silver paint pad for external circuit connection, and then coated with the gel electrolyte, followed by drying in open air overnight. PVA/H_3PO_4 gel electrolyte was prepared by dissolving PVA (10 g) in DI water (100 mL) at 90 °C under stirring. After the mixture became clear and cooled down to room temperature, H_3PO_4 (10 g) was added under stirring.

2.7 Performance tests of FMSCs

The performances of FMSCs were tested in a 2-electrode configuration on the electrochemical workstation (CHI 660E). CV, GCD, and electrochemical impedance spectroscopy (EIS) tests were carried out. The total capacitance (C_{device}) of the two FMSCs was calculated using equation (4) or (5):

$$C_{device} = \frac{Q}{2V} = \frac{1}{2Vv}\int_{V_-}^{V_+} i(V)dV \quad (4)$$

where Q is the total charge obtained by integrating the enclosed area of CV curves, V is the voltage window (V=V_+ - V_-), v is the scan rate of CV curves, and $i(V)$ is the current of CV curves.

$$C_{device} = i/(dV/dt) \quad (5)$$

where i is the discharge current of GCD curves, t is the discharge time and V is the voltage

The specific volumetric capacitance $C_{V,electrode}$ of fiber electrodes in the 2-electrode FMSCs can be calculated using the equation (6):

$C_{V,electrode} = 2C_{device}/V_{electrode}$ (6)

$V_{electrode}$ is the volume of one carbon fiber electrode.

The volumetric capacitance of the FMSCs ($C_{V,device}$) was calculated according to the question (7):

$C_{V,device} = C_{device}/V_{device}$ (7)

V_{device} is the total volume of FMSCs including both electrodes and gel electrolyte.

The volumetric energy density ($E_{V,device}$) of the FMSCs was obtained from equation (8):

$E_{V,device} = \frac{1}{2} C_{V,device} V^2$ (8)

where V is the operating voltage window in volts.

The volumetric power density ($P_{V,device}$) of the FMSCs was calculated using equation (9):

$P_{V,device} = E_{V,device}/t$ (9)

where t is the discharge time.

3. Results and discussion

As illustrated in Fig. 1, GO and MWCNTs were used to form the nanoscale porous sheath. GO sheets used in this study have an average lateral size of ~25 μm (see Fig. S1 in the Supplementary Material (SM). Large GO sheets offer less random alignment leading to a macroscale order when assembled as fibers with an enhanced electrical conductivity and higher mechanical strength compared to fibers produced using small GO sheets [24, 43, 44]. The other component of the sheath, MWCNTs, serves two purposes: (1) preventing the

restacking of GO sheets, to maintain a larger surface area accessible for electrolyte ions, and (2) improving the electrical conductivity of the resulting hybrid. The mass ratio of GO to MWCNTs was set at 4:1 based on the optimization made in our previous studies [29, 30]. Besides, EDA was added to the mixture to reduce and nitrogen-dope GO, as well as to crosslink GO sheets with MWCNTs [29]. The graphite fiber bundle is 10-cm long crossing the whole glass tubes.

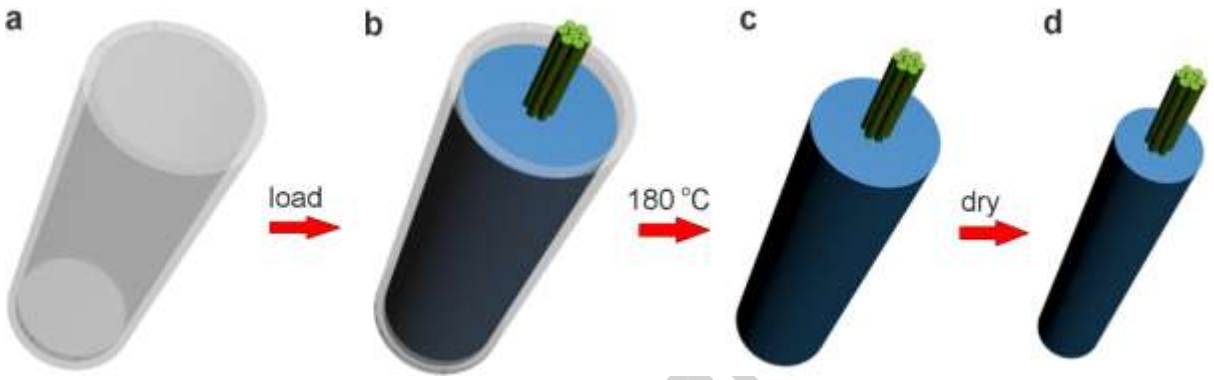

Fig. 1. Schematic illustration of the space-confined hydrothermal assembly of core-sheath fibers. (a) A glass tube sealed at one end. (b) GO/MWCNT/EDA dispersion injected into the glass tube together with a bunch of densely packed commercial graphite fibers. (c) Hydrothermal assembly inside the glass tube at 180 °C in an autoclave. (d) The dried carbon fiber with a graphite fiber core and GO/MWCNT hybrid sheath.

At each run, tens of glass tubes filled with GO/MWCNT/EDA dispersion and graphite fibers were loaded vertically in an autoclave; and the autoclave was heated to the desired hydrothermal condition at 180 °C. We previously studied the formation of GO/MWCNT fibers in capillary channels in different diameters ranging from 0.3 to 2 mm [30]. It was found that larger channels could yield hybrid fibers with higher specific length capacitance, which are beneficial for increasing the energy storage capacity of FMSCs. However, because

of smaller capillary pressure in large diameter channels, the packing density of large diameter hybrid carbon fibers is much smaller than that of smaller fibers, leading to their inferior performances at higher scanning or charge/discharge rates [30]. Thus, in this study, we focused on the synthesis of fiber electrodes using large glass tubes (*i.e.* 2 mm in diameter).

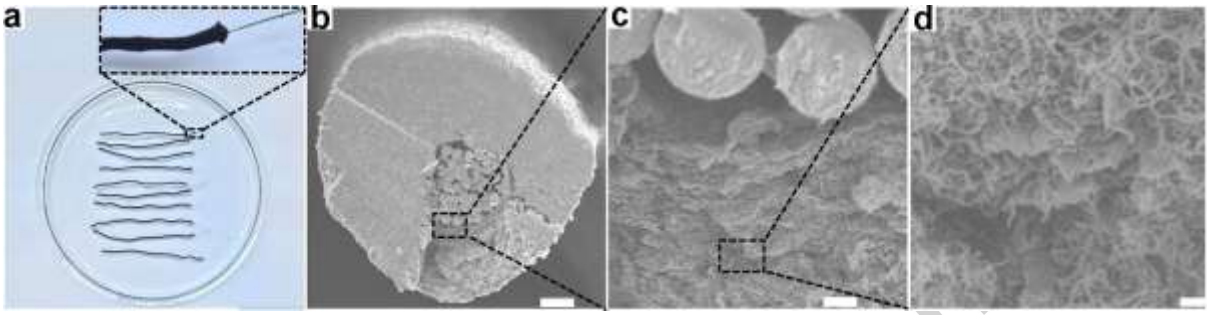

Fig. 2. (a) Photography of core-sheath fibers, the enlarged photo shows one end of the fiber with graphite fibers extending out. (b) Cross-sectional SEM image of the core-sheath fiber and (c, d) SEM images of the enlarged views of sheath layers. Scale bars are 20 μm in (b), 2 μm in (c), and 200 nm in (d). (Note that the interface of commercial carbon fiber core and GO/MWCNT-derived sheath is visible in Fig. 2c in enlarged form.)

Fig. 2a shows a photograph of several as-synthesized core-sheath fibers in water. As displayed in the enlarged photograph, a thick layer of GO/MWCNT-derived sheath is wrapped uniformly around the graphite fiber core. After drying, the sheath shrinks significantly due to capillary forces, and the graphite fiber bundle was packed densely in the middle (see Fig. 2b). It is desirable to keep the volume fraction of graphite fibers small so that the whole fiber can have larger specific volumetric capacitance values. The diameter of dried core-sheath fibers is ~170 μm whereas that of the graphite fiber bundle is ~45 μm. Accordingly, graphite fibers only take up about 7% of the volume of the overall fiber. SEM images in Fig. 2c and 2d show that graphene sheets are closely packed but not restacked

together, which are beneficial to create larger surface area accessible for electrolytes. Further, MWCNTs fill the gaps and voids among graphene sheets and distribute uniformly throughout the sheath. For comparison, the core-free hybrid fibers were also synthesized under the same conditions. They have a larger diameter of ~235 μm after drying (see Fig. S2a and 2b in SM).

The porosity of core-sheath and core-free fibers was studied by measuring their nitrogen adsorption/desorption isotherms, and the results are presented in Fig. S3 in SM. Since the surface area of graphite fiber core is negligible compared to that of the GO/MWCNT sheath. We peeled off the GO/MWCNT sheath from the graphite fiber core to compare with the core-free fibers. Their specific surface areas are similar, with the GO/MWCNT sheath at 264.6 m^2/g and the core-free hybrid fibers at 238.4 m^2/g, respectively. Hysteresis loops on their nitrogen adsorption-desorption isotherms indicate the existence of mesopores, which are beneficial for achieving fast ion transport.

EDS and XPS were used to study the chemical nature of the core-sheath fibers. EDS maps (see Fig. S4 in SM) show that C, O, and N are distributed uniformly throughout the sheath. Correspondingly, their XPS spectra (Fig. S5 in SM) further illustrate chemical structures of C, O, and N in the fibers. Their core-level C 1s peak can be deconvoluted into five sub-peaks. Peaks centered at ~284.0 and ~284.9 eV correspond to carbon atoms in sp^2- and sp^3-hybridized structures, respectively; and peaks at ~286.3, ~287.8, and ~288.9 eV are associated with C-N/C-O, C=O, and O=C-O bonds, respectively [29, 45]. These results reveal that some functional groups still remain after chemical and thermal reduction of oxygen functionalities. In addition to C 1s, the analysis of N 1s region is quite essential, as we also want to N-dope the fiber. The N atomic content is about 4.3%. N1s seen in Fig. S5c can be deconvoluted into three sub-peaks at ~398.2, ~399.6, and ~402.0 eV. The peak at ~398.2 eV corresponds to pyridinic nitrogen and the peak at ~399.6 is associated with amine moieties or other sp^3 carbon and nitrogen bonds. The peak at ~402.0 eV can be ascribed to pyrrolic and

graphitic nitrogen [9, 30, 46]. Overall, EDS and XPS results confirm that we have managed to successfully dope the GO-MWCNT sheaths with nitrogen functionalities, which is in agreement with our previous observations [29, 30].

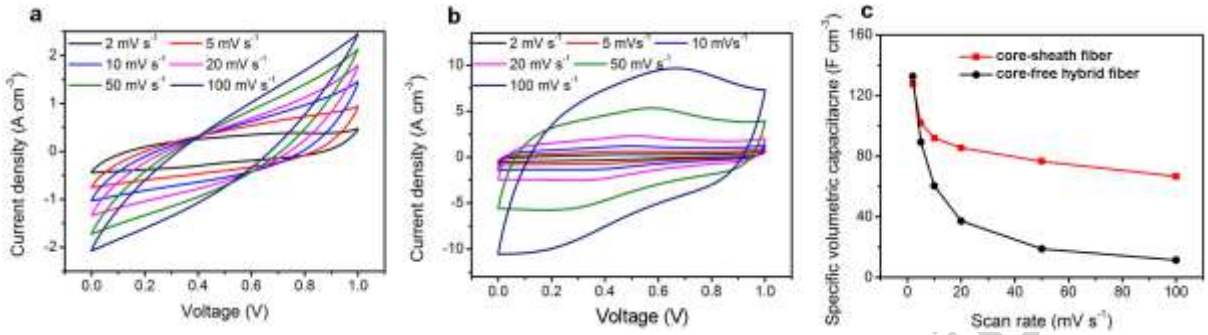

Fig. 3. Electrochemical performances of the GO/MWCNT-derived core-free hybrid fiber and the core-sheath fiber measured using a 3-electrode configuration in 1 M H_2SO_4 electrolyte. Both fibers are cut into ~1 cm in length as working electrodes. (a) CV curves of the core-free fibers (a) and the core-sheath fibers (b) at different scan rates. (c) Specific volumetric capacitances of the two types of fibers at different scan rates calculated from their CV curves.

To evaluate the electrochemical performances of the core-sheath fibers, CV and GCD tests were carried out in a 3-electrode configuration in comparison with the core-free hybrid fibers. Fig. 3a shows that CV curves of the core-free fibers are spindle-shaped, especially at higher scan rates, suggesting a slow charge transfer rate. Correspondingly, their GCD curves (Fig. S6a in SM) exhibit large voltage drops at the beginning of the discharge process, indicating their low electrical conductivity. In contrast, the CV curves of the core-sheath fibers (Fig. 3b) maintain quasi-rectangular shapes with large enclosed areas at high scan rates up to 100 mV s^{-1}, indicating their much better rate capability as electrodes for FMSCs. This can also be observed in their GCD curves (Fig. S6b in SM) with much smaller voltage drops as compared to those of core-free hybrid fibers. Their specific volumetric capacitances at different scan

rates were calculated from their CV curves. The results are summarized in Fig. 3c. Because graphite fiber cores may have only a limited contribution to the total capacitance, the specific volumetric capacitance of the core-sheath fiber is slightly smaller than that of the core-free fibers at the scan rate of 2 mV s^{-1}. However, with the increase in scan rate, the specific volumetric capacitance of the core-sheath fiber becomes much larger than that of core-free fibers above 5 mV s^{-1}. From 2 to 100 mV s^{-1}, the core-sheath fiber preserves more than 52% of its initial capacitance, which is six times higher compared to that of the core-free hybrid fiber keeps at 8.5%. The significantly improved rate capacity can be attributed to its conductive graphite fiber core with an electrical conductivity of ~680 S cm^{-1}, which is much larger than that of the core-free hybrid fiber (*i.e.* ~23 S cm^{-1}). Thus, as expected, the charge transfer is much more efficient through the graphite fiber core.

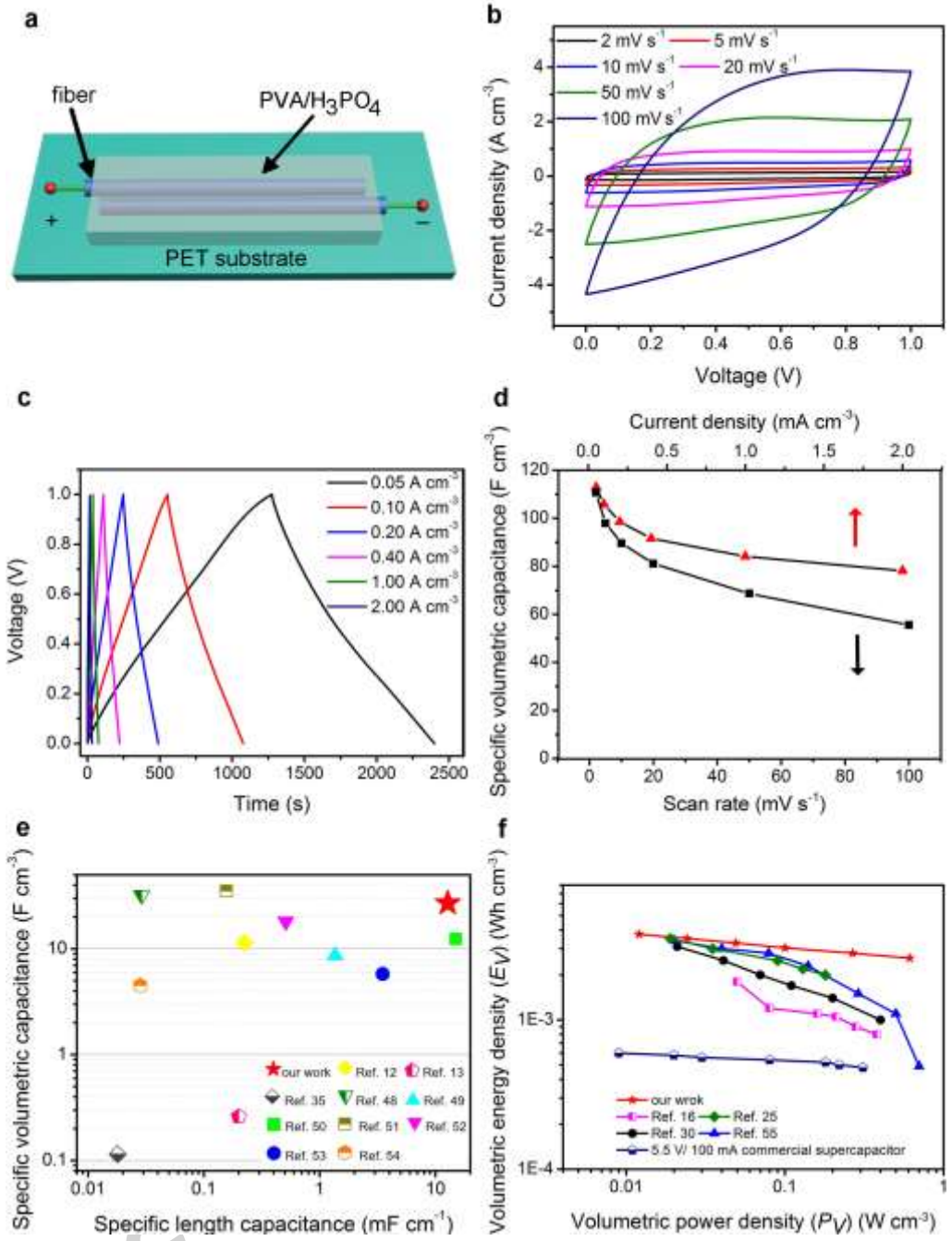

Fig. 4. Performances of a symmetric all-solid-state FMSC assembled using two core-sheath fibers. (a) Schematic illustration of the FMSC assembled by two core-sheath fibers of ~1 cm in length in PVA/H_3PO_4 gel electrolyte on a PET substrate. (b) CV curves of the FMSC at different scan rates. (c) GCD curves of the FMSC at different charge/discharge current densities. (d) The specific volumetric capacitance of each fiber electrode of the FMSC at different scan rates and charge/discharge current densities. (e) Comparison of the specific

length and volumetric capacitance of the FMSC in this study with those reported in previous literatures. (f) Comparison of the energy and power densities of the FMSC in this study with those reported in previous literatures.

Next, a solid-state FMSC was fabricated using the core-sheath fibers as fiber electrodes. As illustrated in Fig. 4a, two core-sheath fibers of ~1 cm in length were assembled into a symmetric FMSC using PVA/H_3PO_4 as a gel electrolyte. Fig. 4b shows that CV curves of this FMSC retain a quasi-rectangular shape at the high scan rate up to 100 mV s^{-1}, indicating fast charge transfer in its electrodes. Correspondingly, its GCD curves in Fig. 4c have a symmetric triangular-shape at the charge/discharge current density from 0.05 to 2 A cm^{-1}. The specific volumetric capacitance of each electrode of the FMSC was calculated from both CV and GCD curves, and the results are presented in Fig. 4d. It should be noted that capacitances calculated from CV depend on voltage scan rates, while those of GCD depend on current densities applied. Thus, the specific volumetric capacitances of each electrode obtained from CV and GCD curves are not exactly marching to each other. The specific volumetric capacitances vary from 112.7, 105.7, 98.6, 91.6, 84.1 to 78.4 F cm^{-3} when the discharge current density increases from 0.05, 0.1, 0.2, 0.4, 1.0 to 2.0 A cm^{-3}. This FMSC can retain above 69% of its initial specific volumetric capacitance from 0.05 to 2.0 A cm^{-3} which is superior to many previously reported fiber based FMSCs with fiber electrodes in similar diameters, such as those made of wet-spun graphene fibers (100 μm in diameter) [47], wet-spun graphene fibers with a sheath of carboxymethyl cellulose (75 μm in diameter) [25] and nitrogen-doped GO/MWCNT fibers (236 ± 10 μm in diameter) [30].

The total volume of this FMSC including both electrodes and the surrounding gel electrolyte is ~4.74 × 10^{-4} cm^3/cm in length. Thus, the specific length capacitance and specific volumetric capacitance of the FMSC were calculated to be 12.8 mF cm^{-1} and 27 F

cm^{-3}, respectively, at the current density of 0.05 A cm^{-3}. These performances are higher than many recent reported performance results of FMSCs [12, 13, 35, 48-54]. Their comparison is shown in Fig. 4e. The details of previous studies and their measurement conditions are listed in Table S1 in SM. The specific volumetric energy and power densities of the FMSC were calculated from its GCD curves, and the results are shown in Fig. 4f. It achieves a high energy density of 3.75 mWh cm^{-3} at the power density of 12 mW cm^{-3}, and retains a high energy density of 2.60 mWh cm^{-3} at the high power density of 612 mW cm^{-3}. These performance data are higher than those of a 5.5-V/100-mF commercial SC, and are one of the best among recently reported FMSCs, such as those made of rGO/MnO_2 nanosheets/polypyrrole deposited on stainless steel current collector (1.1 mWh cm^{-3}, 150 mW cm^{-3}) [50], rGO@carboxymethyl cellulose core-sheath structured fiber (3.5 mWh cm^{-3}, 180 mW cm^{-3}) [25], MWCNT/rGO fiber (3.4 mWh cm^{-3}, 700 mW cm^{-3}) [55] and nitrogen-doped rGO/MWCNT fiber (3.1 mWh cm^{-3}, 400 mW cm^{-3}) [30]. It should be noted that many previously reported FMSCs could achieve a high energy density at low power densities. But they suffer from a significant drop in energy density with the increase of power densities, which limits their application potential. In contrast, the FMSC reported in this study can retain up to 69.3% of their initial energy density when its power density increases over fifty times, from 12 to 612 mWh cm^{-3}. This is promising to develop practical high-performance FMSCs that will be useful for various WEDs.

The stability of the FMSC was evaluated by the CV at 100 mV s^{-1} for 10000 cycles. Fig. 5a shows that the FMSC retains ~96.5% of its initial capacitance even after 10000 cycles, indicating excellent cycling stability. To evaluate its mechanical stability, the FMSC was fully bent (*i.e.* ~180°) for 1000 times. The FMSC can retain its structural integrity after bending, and remarkably shows only ~0.1% of drop in its capacitance at 100 mV s^{-1}, which suggests excellent mechanical stability (Fig. 5b). The capacitance retention was also

monitored by the CV at 100 mV s^{-1} for 10000 cycles when the FMSC was bent at ~180°. Fig. S7 in SM shows that it retains ~95.2% of its initial capacitance.

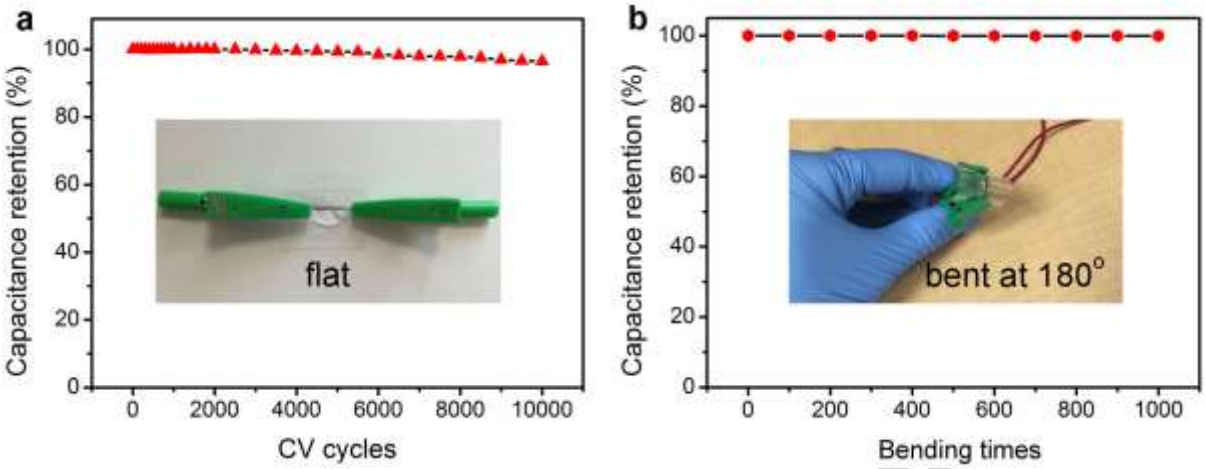

Fig. 5. (a) Cycling tests of the FMSC at the scan rate of 100 mV s^{-1} for 100000 cycles. (Inset is a photograph of the FMSC). (b) Capacitance retention test of the FMSC when bent at 180° for 1000 times. (Inset photograph shows the fully bent FMSC.)

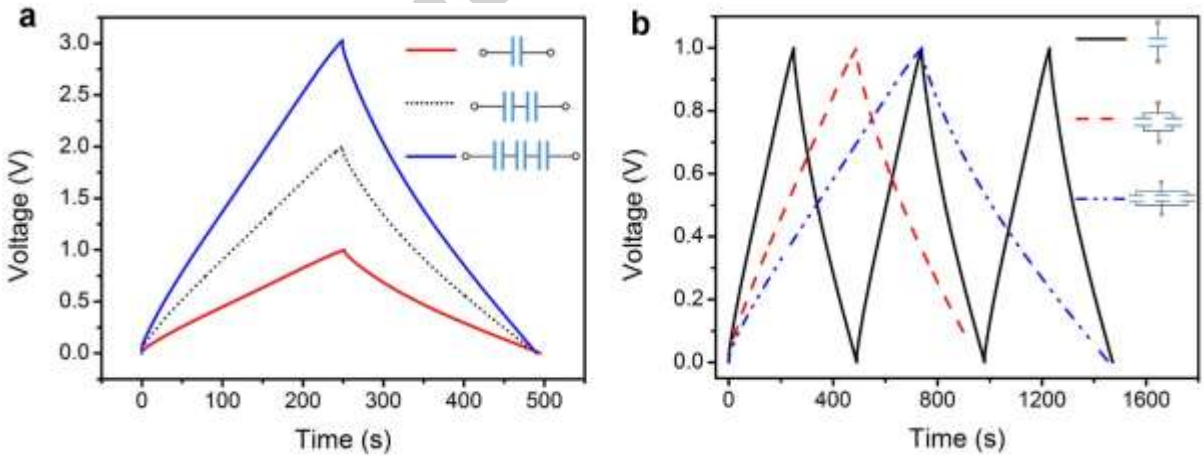

Fig. 6. GCD curves of one, two or three FMSCs connected in series (a) and in parallel (b). (Note that the inset images show corresponding integration schematics in both figures)

For practical WED applications, it is desirable to connect FMSCs in series or parallel to broaden their operating voltage and current. Fig. 6a shows that when two or three FMSCs are connected in series, their charge/discharge voltage windows are expanded to 2 and 3 V, respectively, without changing discharge time. Fig. 6b exhibits that when two or three FMSCs are connected in parallel, their output currents are doubled and tripled, respectively, with the same voltage window. Both results demonstrate the excellent integratability and scalability of the FMSCs assembled using core-sheath fibers.

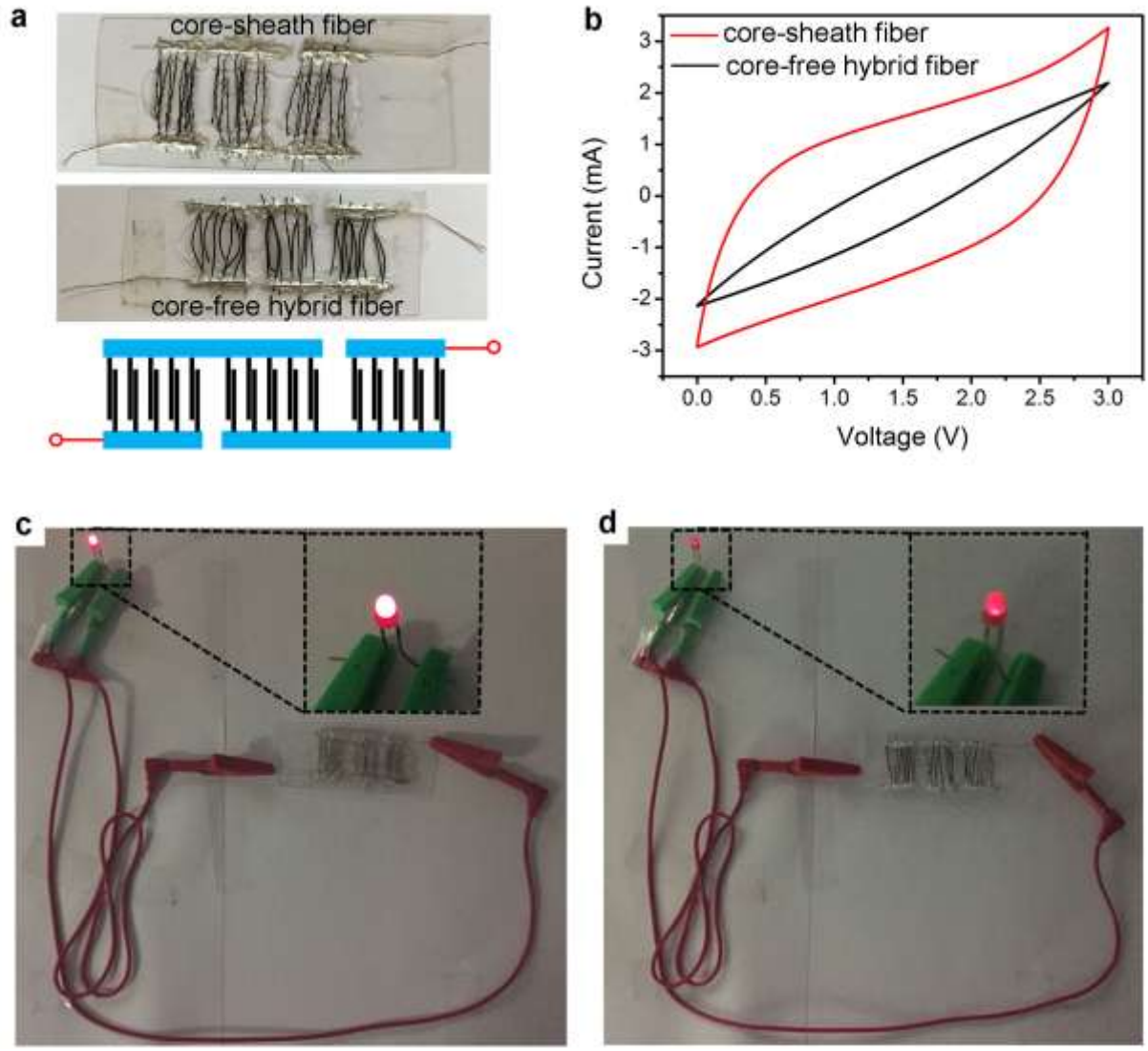

Fig. 7. (a) Photography of two energy storage units, integrated by the core-sheath fiber based FMSCs (upper), core-free hybrid fiber based FMSCs (middle) and their corresponding

integration schematics (bottom): five FMSCs are integrated into a parallel array first, and then three parallel arrays are connected in series. (b) CV curves of the two energy storage units. Photography of a LED lightened by the energy storage unit integrated by the core-sheath fiber based FMSCs (c) and the core-free hybrid fiber based FMSCs (d).

To further demonstrate the potential for practical applications, as shown in Fig. 7a, the energy storage unit was fabricated by integrating fifteen fibers together, with five connected in parallel first into the parallel array and then three parallel arrays were assembled in series. For comparison, we also fabricated another energy storage unit using the core-free fibers. Fig. 7b shows the CV curves of the two energy storage units at the scan rate of 200 mV s^{-1}. The CV curve of the energy storage unit assembled from the core-sheath fibers has a much larger enclose area and a more rectangular shape, indicating faster charge transfer and more energy stored. The energy storage unit integrated by core-sheath fibers has the energy density of 2.54 mWh cm^{-3} at the power density of 121.14 mW cm^{-3}. In contrast, the unit integrated by core-free hybrid fibers can only deliver the energy density of 1.17 mWh cm^{-3} at the power density of 65.22 mW cm^{-3}. We used them to light a red LED to further compare their performances. Both were first charged at the same current intensity (3 mA). The energy storage unit assembled from the core-sheath fibers can light the red LED for 3 minutes (see Fig. 7c and a video clip in SM) whereas the other unit can only power the same LED for around 1.5 minutes (see Fig. 7d and a video clip in SM). Besides, the LED powered by the energy storage unit assembled from the core-sheath fibers is much brighter. Furthermore, the energy strorage unit can also work under bending, twisting and stretching conditions as shown in Fig. S8 in SM.

4. Conclusions

Novel micro-nano-integrated core-sheath fibers were synthesized by space-confined hydrothermal assembly of nitrogen doped GO/MWCNT hybrids around commercial graphite fiber cores. The nanoscale GO/MWCNT hybrids provide large surface area (up to 400 m^2/g) and sufficient surface functional groups (4.3% of N) for capacitive energy storage. The microscale graphite fiber core with high electrical conductivity (680 S cm^{-1}) serves as fast electron transfer pathways. As a result, the core-sheath fiber preserves more than 52% of its initial capacitance from 2 to 100 mV s^{-1}, more than six times increase in rate capability compared to that of the core-free hybrid fiber. All-solid-state FMSCs assembled using these fiber electrodes show a high specific length capacitance of 12.8 mF cm^{-1} and a high specific volumetric capacitance of 27 F cm^{-3} at the current density of 0.05 A cm^{-3}. They can retain ~69.3% of their initial capacitances when the current density increases from 0.05 to 2 A cm^{-3}. They also exhibit the high energy density of 3.75 mWh cm^{-3} at the power density of 12 mW cm^{-3}, and can retain an energy density of 2.60 mWh cm^{-3} at the high power density of 612 mWh, which are higher than most of previously reported FMSCs. The FMSC in this study also show good long-term stability with the capacitance retention of ~96.5% after 10000 cycles, and excellent mechanical stability with ~99.9% capacitance retention after 1000 bending cycles. Furthermore, multiple FMSCs can be assembled in parallel and/or in series to expand their working voltage window or/and current densities. An integrated energy storage unit comprising of 15 FMSCs was assembled to lighten an LED indicator, demonstrating its good potential in WED applications.

Acknowledgements

Appendix A. Supplementary material

Supplementary data associated with this article can be found in the online version at **

References

[1] S. Coyle, Y.Z. Wu, K.T. Lau, D. De Rossi, G. Wallace, D. Diamond, Smart nanotextiles: A review of materials and applications, MRS Bull., 32 (2007) 434-442.

[2] M. Stoppa, A. Chiolerio, Wearable electronics and smart textiles: a critical review, Sensors, 14 (2014) 11957-11992.

[3] C. Xia, W. Chen, X. Wang, M.N. Hedhili, N. Wei, H.N. Alshareef, Highly Stable Supercapacitors with Conducting Polymer Core-Shell Electrodes for Energy Storage Applications, Adv. Energy Mater., 5 (2015) 1401805.

[4] D. Yu, Q. Qian, L. Wei, W. Jiang, K. Goh, J. Wei, J. Zhang, Y. Chen, Emergence of fiber supercapacitors, Chem. Soc. Rev., 44 (2015) 647-662.

[5] W. Jiang, D. Yu, Q. Zhang, K. Goh, L. Wei, Y. Yong, R. Jiang, J. Wei, Y. Chen, Ternary Hybrids of Amorphous Nickel Hydroxide–Carbon Nanotube-Conducting Polymer for Supercapacitors with High Energy Density, Excellent Rate Capability, and Long Cycle Life, Adv. Energy Mater., 25 (2015) 1063-1073.

[6] N. Li, Z. Chen, W. Ren, F. Li, H.-M. Cheng, Flexible graphene-based lithium ion batteries with ultrafast charge and discharge rates, PNAS, 109 (2012) 17360-17365.

[7] Y.H. Kwon, S.W. Woo, H.R. Jung, H.K. Yu, K. Kim, B.H. Oh, S. Ahn, S.Y. Lee, S.W. Song, J. Cho, Cable-type flexible lithium ion battery based on hollow multi-helix electrodes, Adv. Mater., 24 (2012) 5192-5197.

[8] H. Nishide, K. Oyaizu, Toward flexible batteries, Science, 319 (2008) 737-738.

[9] B. Liu, J. Zhang, X. Wang, G. Chen, D. Chen, C. Zhou, G. Shen, Hierarchical three-dimensional ZnCo2O4 nanowire arrays/carbon cloth anodes for a novel class of high-performance flexible lithium-ion batteries, Nano Lett., 12 (2012) 3005-3011.

[10] G. Zhou, F. Li, H.-M. Cheng, Progress in flexible lithium batteries and future prospects, Energy Environ. Sci., 7 (2014) 1307-1338.

[11] B. Zheng, T. Huang, L. Kou, X. Zhao, K. Gopalsamy, C. Gao, Graphene fiber-based asymmetric micro-supercapacitors, J. Mater. Chem. A, 2 (2014) 9736-9743.

[12] Y. Liang, Z. Wang, J. Huang, H. Cheng, F. Zhao, Y. Hu, L. Jiang, L. Qu, Series of in-fiber graphene supercapacitors for flexible wearable devices, J. Mater. Chem. A, 3 (2015) 2547-2551.

[13] J. Bae, M.K. Song, Y.J. Park, J.M. Kim, M. Liu, Z.L. Wang, Fiber Supercapacitors Made of Nanowire-Fiber Hybrid Structures for Wearable/Flexible Energy Storage, Angew. Chem. Int. Ed., 50 (2011) 1683-1687.

[14] M. Beidaghi, Y. Gogotsi, Capacitive energy storage in micro-scale devices: recent advances in design and fabrication of micro-supercapacitors, Energy Environ. Sci., 7 (2014) 867-884.

[15] D. Yu, K. Goh, Q. Zhang, L. Wei, H. Wang, W. Jiang, Y. Chen, Controlled Functionalization of Carbonaceous Fibers for Asymmetric Solid-State Micro-Supercapacitors with High Volumetric Energy Density, Adv. Mater., 26 (2014) 6790-6797.

[16] Y. Huang, M. Zhu, Y. Huang, H. Li, Z. Pei, Q. Xue, Z. Liao, Z. Wang, C. Zhi, A modularization approach for linear-shaped functional supercapacitors, J. Mater. Chem. A, 4 (2016) 4580-4586.

[17] X. Xiao, T. Li, P. Yang, Y. Gao, H. Jin, W. Ni, W. Zhan, X. Zhang, Y. Cao, J. Zhong, Fiber-based all-solid-state flexible supercapacitors for self-powered systems, Acs Nano, 6 (2012) 9200-9206.

[18] J. Ren, L. Li, C. Chen, X. Chen, Z. Cai, L. Qiu, Y. Wang, X. Zhu, H. Peng, Twisting Carbon Nanotube Fibers for Both Wire-Shaped Micro-Supercapacitor and Micro-Battery, Adv. Mater., 25 (2013) 1155-1159.

[19] K.S. Novoselov, A.K. Geim, S. Morozov, D. Jiang, Y. Zhang, S.a. Dubonos, I. Grigorieva, A. Firsov, Electric field effect in atomically thin carbon films, science, 306 (2004) 666-669.

[20] D. Chen, L. Tang, J. Li, Graphene-based materials in electrochemistry, Chem. Soc. Rev., 39 (2010) 3157-3180.

[21] C.e.N.e.R. Rao, A.e.K. Sood, K.e.S. Subrahmanyam, A. Govindaraj, Graphene: the new two-dimensional nanomaterial, Angew. Chem. Int. Ed., 48 (2009) 7752-7777.

[22] T. Lin, I.-W. Chen, F. Liu, C. Yang, H. Bi, F. Xu, F. Huang, Nitrogen-doped mesoporous carbon of extraordinary capacitance for electrochemical energy storage, Science, 350 (2015) 1508-1513.

[23] C. Lee, X. Wei, J.W. Kysar, J. Hone, Measurement of the elastic properties and intrinsic strength of monolayer graphene, science, 321 (2008) 385-388.

[24] Z. Xu, H. Sun, X. Zhao, C. Gao, Ultrastrong fibers assembled from giant graphene oxide sheets, Adv. Mater., 25 (2013) 188-193.

[25] L. Kou, T. Huang, B. Zheng, Y. Han, X. Zhao, K. Gopalsamy, H. Sun, C. Gao, Coaxial wet-spun yarn supercapacitors for high-energy density and safe wearable electronics, Nat. Commun., 5 (2014) 3754.

[26] G. Xin, T. Yao, H. Sun, S.M. Scott, D. Shao, G. Wang, J. Lian, Highly thermally conductive and mechanically strong graphene fibers, Science, 349 (2015) 1083-1087.

[27] Z. Dong, C. Jiang, H. Cheng, Y. Zhao, G. Shi, L. Jiang, L. Qu, Facile fabrication of light, flexible and multifunctional graphene fibers, Adv. Mater., 24 (2012) 1856-1861.

[28] X. Ding, Y. Zhao, C. Hu, Y. Hu, Z. Dong, N. Chen, Z. Zhang, L. Qu, Spinning fabrication of graphene/polypyrrole composite fibers for all-solid-state, flexible fibriform supercapacitors, J. Mater. Chem. A, 2 (2014) 12355-12360.

[29] D. Yu, K. Goh, H. Wang, L. Wei, W. Jiang, Q. Zhang, L. Dai, Y. Chen, Scalable synthesis of hierarchically structured carbon nanotube-graphene fibres for capacitive energy storage, Nat. Nanotechnol., 9 (2014) 555-562.

[30] W. Jiang, S. Zhai, Q. Qian, Y. Yuan, H.E. Karahan, L. Wei, K. Goh, A.K. Ng, J. Wei, Y. Chen, Space-confined assembly of all-carbon hybrid fibers for capacitive energy storage: realizing a built-to-order concept for micro-supercapacitors, Energy Environ. Sci., (2016) 611-622.

[31] R. Cruz-Silva, A. Morelos-Gomez, H.-i. Kim, H.-k. Jang, F. Tristan, S. Vega-Diaz, L.P. Rajukumar, A.L. Elías, N. Perea-Lopez, J. Suhr, Super-stretchable graphene oxide macroscopic fibers with outstanding knotability fabricated by dry film scrolling, ACS nano, 8 (2014) 5959-5967.

[32] J. Carretero–González, E. Castillo–Martínez, M. Dias–Lima, M. Acik, D.M. Rogers, J. Sovich, C.S. Haines, X. Lepró, M. Kozlov, A. Zhakidov, Oriented Graphene Nanoribbon Yarn and Sheet from Aligned Multi-Walled Carbon Nanotube Sheets, Adv. Mater., 24 (2012) 5695-5701.

[33] X. Li, T. Zhao, K. Wang, Y. Yang, J. Wei, F. Kang, D. Wu, H. Zhu, Directly drawing self-assembled, porous, and monolithic graphene fiber from chemical vapor deposition grown graphene film and its electrochemical properties, Langmuir, 27 (2011) 12164-12171.

[34] B.E. Conway, Electrochemical Supercapacitors: Scientific Fundamentals and Technological Applications, Kluwer Academic/Plenum, New York, 1999.

[35] Y. Meng, Y. Zhao, C. Hu, H. Cheng, Y. Hu, Z. Zhang, G. Shi, L. Qu, All-Graphene Core-Sheath Microfibers for All-Solid-State, Stretchable Fibriform Supercapacitors and Wearable Electronic Textiles, Adv. Mater., 25 (2013) 2326-2331.

[36] J.A. Lee, M.K. Shin, S.H. Kim, H.U. Cho, G.M. Spinks, G.G. Wallace, M.D. Lima, X. Lepró, M.E. Kozlov, R.H. Baughman, Ultrafast charge and discharge biscrolled yarn supercapacitors for textiles and microdevices, Nat. Commun., 4 (2013) 1970.

[37] Y. Fu, X. Cai, H. Wu, Z. Lv, S. Hou, M. Peng, X. Yu, D. Zou, Fiber supercapacitors utilizing pen ink for flexible/wearable energy storage, Adv. Mater., 24 (2012) 5713-5718.

[38] Z. Zhang, X. Chen, P. Chen, G. Guan, L. Qiu, H. Lin, Z. Yang, W. Bai, Y. Luo, H. Peng, Integrated polymer solar cell and electrochemical supercapacitor in a flexible and stable fiber format, Adv. Mater., 26 (2014) 466-470.

[39] S. Zhai, H.E. Karahan, L. Wei, Q. Qian, A.T. Harris, A.I. Minett, S. Ramakrishna, A.K. Ng, Y. Chen, Textile energy storage: Structural design concepts, material selection and future perspectives, Energy Storage Materials, 3 (2016) 123-139.

[40] S. Zhai, W. Jiang, L. Wei, H.E. Karahan, Y. Yuan, A.K. Ng, Y. Chen, All-carbon solid-state yarn supercapacitors from activated carbon and carbon fibers for smart textiles, Mater. Horiz., 2 (2015) 598-605.

[41] S.H. Aboutalebi, A.T. Chidembo, M. Salari, K. Konstantinov, D. Wexler, H.K. Liu, S.X. Dou, Comparison of GO, GO/MWCNTs composite and MWCNTs as potential electrode materials for supercapacitors, Energy Environ. Sci., 4 (2011) 1855-1865.

[42] S.H. Aboutalebi, M.M. Gudarzi, Q.B. Zheng, J.K. Kim, Spontaneous formation of liquid crystals in ultralarge graphene oxide dispersions, Adv. Funct. Mater., 21 (2011) 2978-2988.

[43] C. Xiang, C.C. Young, X. Wang, Z. Yan, C.C. Hwang, G. Cerioti, J. Lin, J. Kono, M. Pasquali, J.M. Tour, Large flake graphene oxide fibers with unconventional 100% knot efficiency and highly aligned small flake graphene oxide fibers, Adv. Mater., 25 (2013) 4592-4597.

[44] L. Chen, Y. He, S. Chai, H. Qiang, F. Chen, Q. Fu, Toward high performance graphene fibers, Nanoscale, 5 (2013) 5809-5815.

[45] J. Shen, A. Liu, Y. Tu, H. Wang, R. Jiang, J. Ouyang, Y. Chen, Asymmetric deposition of manganese oxide in single walled carbon nanotube films as electrodes for flexible high frequency response electrochemical capacitors, Electrochim. Acta, 78 (2012) 122-132.

[46] J. Lin, C. Zhang, Z. Yan, Y. Zhu, Z. Peng, R.H. Hauge, D. Natelson, J.M. Tour, 3-dimensional graphene carbon nanotube carpet-based microsupercapacitors with high electrochemical performance, Nano Lett., 13 (2012) 72-78.

[47] T. Huang, B. Zheng, L. Kou, K. Gopalsamy, Z. Xu, C. Gao, Y. Meng, Z. Wei, Flexible high performance wet-spun graphene fiber supercapacitors, RSC Adv., 3 (2013) 23957-23962.

[48] X. Chen, L. Qiu, J. Ren, G. Guan, H. Lin, Z. Zhang, P. Chen, Y. Wang, H. Peng, Novel electric double-layer capacitor with a coaxial fiber structure, Adv. Mater., 25 (2013) 6436-6441.

[49] C. Choi, H.J. Sim, G.M. Spinks, X. Lepró, R.H. Baughman, S.J. Kim, Elastomeric and Dynamic MnO2/CNT Core–Shell Structure Coiled Yarn Supercapacitor, Adv. Energy Mater., (2016).

[50] Y. Huang, H. Hu, Y. Huang, M. Zhu, W. Meng, C. Liu, Z. Pei, C. Hao, Z. Wang, C. Zhi, From industrially weavable and knittable highly conductive yarns to large wearable energy storage textiles, ACS nano, 9 (2015) 4766-4775.

[51] P. Xu, B. Wei, Z. Cao, J. Zheng, K. Gong, F. Li, J. Yu, Q. Li, W. Lu, J.-H. Byun, Stretchable wire-shaped asymmetric supercapacitors based on pristine and MnO2 coated carbon nanotube fibers, ACS nano, 9 (2015) 6088-6096.

[52] Y. Zhang, W. Bai, X. Cheng, J. Ren, W. Weng, P. Chen, X. Fang, Z. Zhang, H. Peng, Flexible and Stretchable Lithium-Ion Batteries and Supercapacitors Based on Electrically Conducting Carbon Nanotube Fiber Springs, Angew. Chem. Int. Ed., 126 (2014) 14792-14796.

[53] H. Jin, L. Zhou, C.L. Mak, H. Huang, W.M. Tang, H.L.W. Chan, High-performance fiber-shaped supercapacitors using carbon fiber thread (CFT)@ polyanilne and functionalized CFT electrodes for wearable/stretchable electronics, Nano Energy, 11 (2015) 662-670.

[54] B. Wang, X. Fang, H. Sun, S. He, J. Ren, Y. Zhang, H. Peng, Fabricating Continuous Supercapacitor Fibers with High Performances by Integrating All Building Materials and Steps into One Process, Adv. Mater., 27 (2015) 7854-7860.

[55] Y. Ma, P. Li, J.W. Sedloff, X. Zhang, H. Zhang, J. Liu, Conductive graphene fibers for wire-shaped supercapacitors strengthened by unfunctionalized few-walled carbon nanotubes, ACS nano, 9 (2015) 1352-1359.

Supplementary material

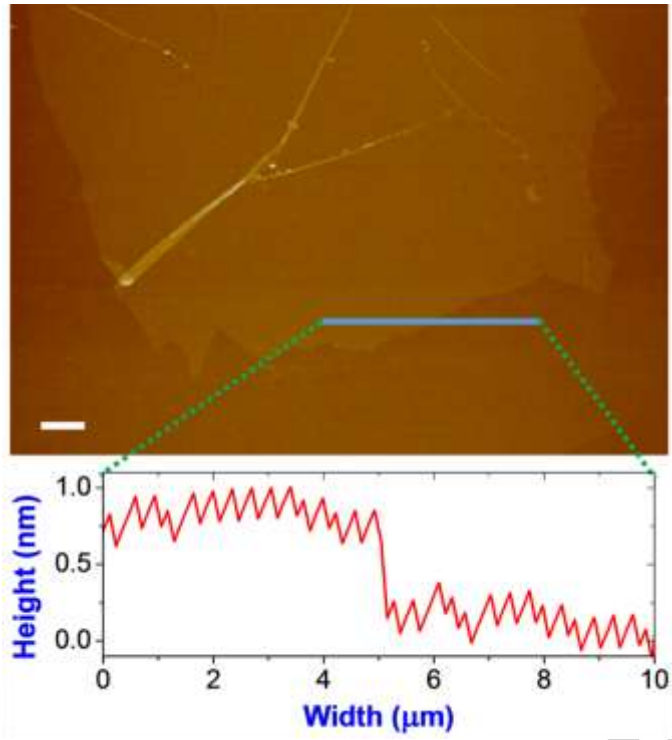

Fig. S1. An atomic force microscope image of GO sheets used in this study and its corresponding height profile. (Scale bar: 2 μm.)

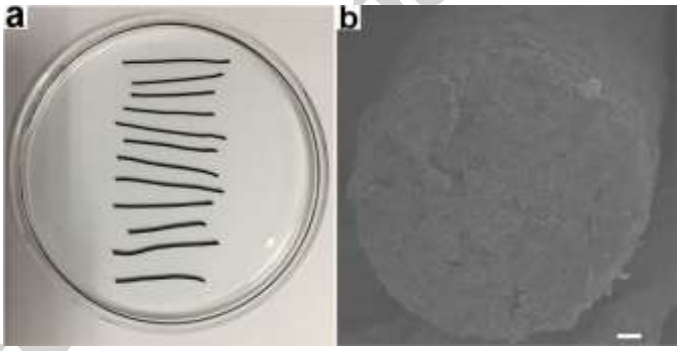

Fig. S2. (a) Photography of (core-free) GO/MWCNT-derived hybrid fibers. (b) Scanning electron microscope (SEM) image of the cross-section of a GO/MWCNT-derived hybrid fiber. (Scale bar: 20 μm.)

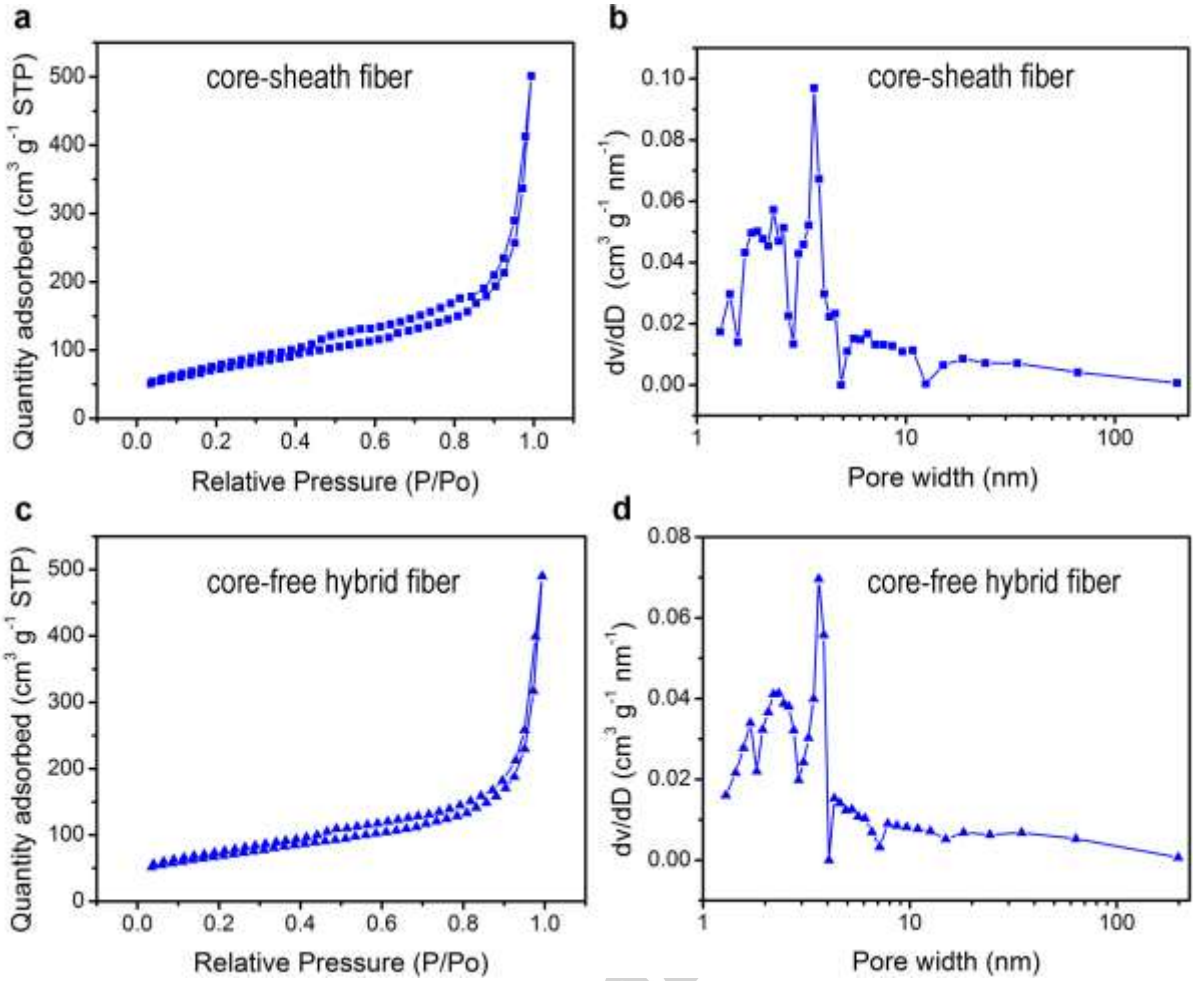

Fig. S3. (a) Nitrogen adsorption/desorption isotherm and (b) pore size distribution of core-sheath fibers (graphite fiber core was removed). (c) Nitrogen adsorption/desorption isotherm and (d) pore size distribution of core-free hybrid fibers.

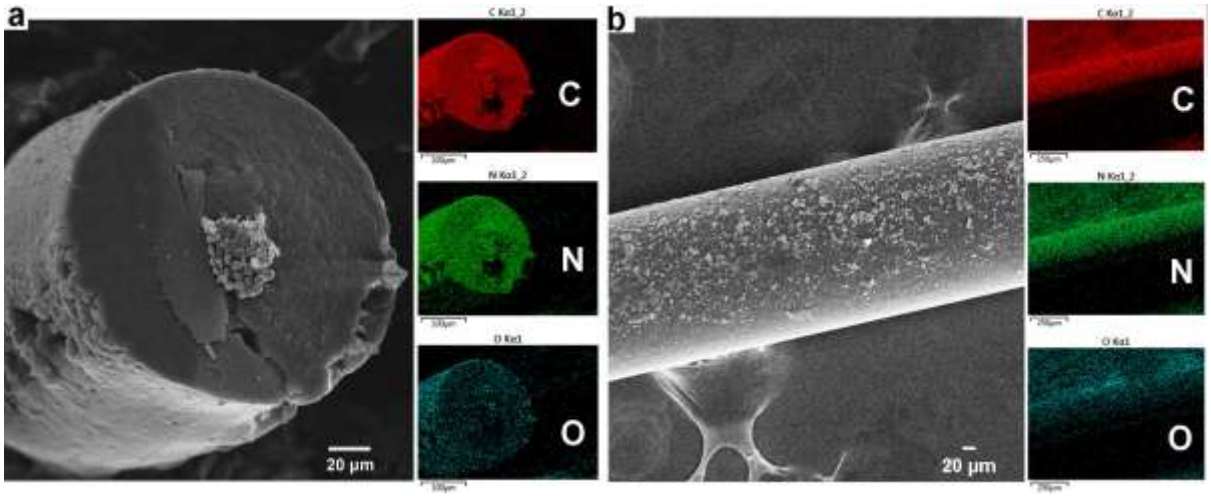

Fig. S4. (a) SEM image of the cross-section of a core-sheath fiber and its corresponding EDS maps for C, O, and N. (b) SEM image of a core-free fiber and its corresponding EDS maps for C, O, and N.

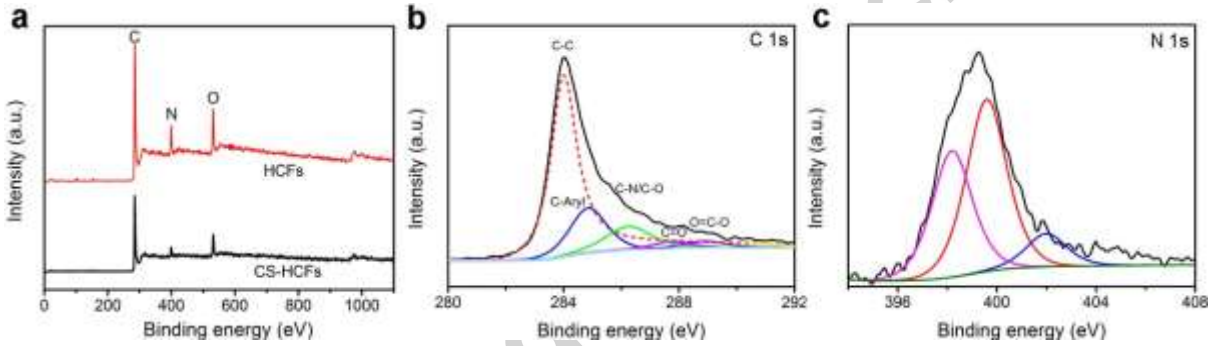

Fig. S5. (a) XPS spectra of the core-free and core-sheath fibers. (b) C1s XPS peak and (c) N1s XPS peak of the core-sheath fiber.

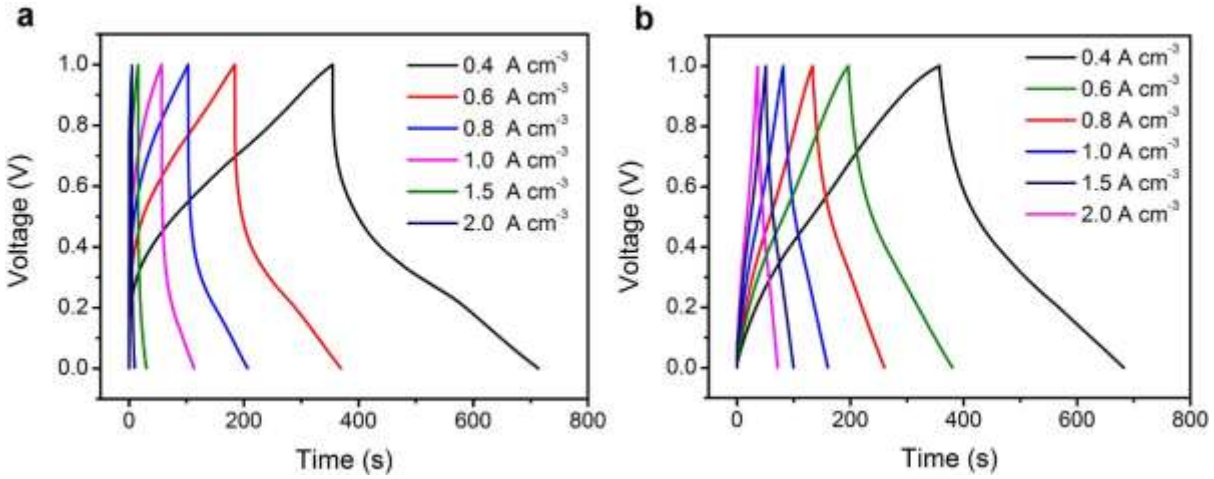

Fig. S6. Electrochemical performances of core-free and core-sheath fibers measured using a 3-electrode configuration in 1 M H_2SO_4 electrolyte. Both fibers are cut into 1 cm in length as working electrodes. GCD curves of (a) core-free and (b) core-sheath fibers at different charge/discharge current densities.

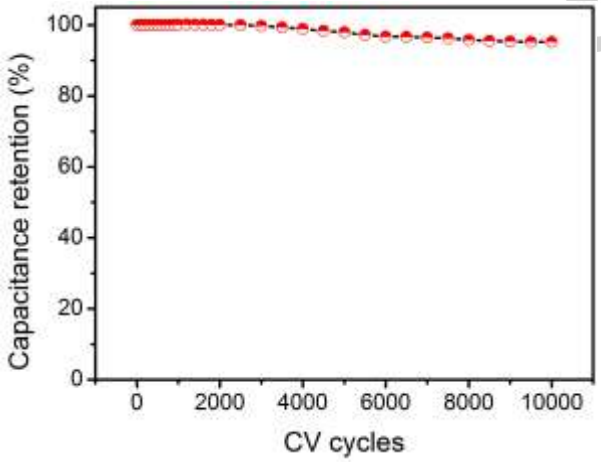

Fig. S7. Capacitance retention test of the FMSC when bent at 180° for 10000 times.

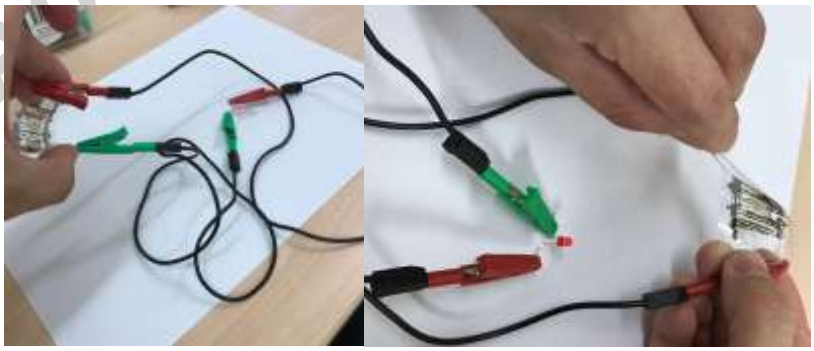

Fig. S8. Photography shows that the integrated energy storage unit can work under bending, twisting and stretching conditions.

Table S1 Comparison of fiber supercapacitors reported in the literature. (All measurements given are based on 2-electrode method.)

* These values are based on the actual devices built. # Reference number is same as that of main text.

References[#]	**Electrode materials**	**Diameter (electrode) (μm)**	**Electrolyte**	**Specific length capacitance* ($mF\ cm^{-1}$)**	**Specific volumetric capacitance* ($F\ cm^{-3}$)**
This work	N-GO/MWCNT core-sheath fiber	170	PVA/H_3PO_4	12.8	27.00
48	CNT sheets / CNT fiber	43*	PVA/H_3PO_4	0.029	32.09
35	3D porous network-like graphene framework / graphene fiber	100	PVA/H_2SO_4	0.018	0.115
49	MnO_2/CNT fibers	80	PVA/LiCl	1.36	8.65
54	CNT fibers	20	PVA/H_3PO_4	0.02826	4.5
13	ZnO nanowires / Plastic wires	220	PVA/H_3PO_4	0.2	0.26
53	PANI coated carbon fiber thread / functionalized carbon fiber thread		PVA/H_3PO_4	3.5	5.8
12	rGO-GO	50	electrolyte free	0.225	11.44
52	CNT fibers	65	PVA/H_2SO_4	0.51	18.12
51	MnO_2 / CNT fiber	31	PVA/KOH	0.157	35.19
50	PPy / MnO_2 / rGO	180-250	PVA/H_3PO_4	15	12.4